Nanostructured Nitrogen Doped Diamond for the Detection of Toxic Metal Ions

Sujit Deshmukh[1], Kamatchi Jothiramalingam Sankaran[2,3], Svetlana Korneychuk,[4] Johan Verbeeck,[4] James Mclaughlin, [5] Ken Haenen[2, 3] and Susanta Sinha Roy[*1]

[1]Department of Physics, School of Natural Sciences, Shiv Nadar University, NH-91, Uttar Pradesh 201314, India.

[2]Institute for Materials Research (IMO), Hasselt University, 3590 Diepenbeek, Belgium.

[3]IMOMEC, IMEC vzw, 3590 Diepenbeek, Belgium.

[4]Electron Microscopy for Materials Science (EMAT), University of Antwerp, 2020 Antwerp, Belgium.

[5]Nanotechnology and Integrated Bioengineering Centre, University of Ulster, Jordanstown Campus, Newtownabbey, BT37 0QB, Northern Ireland, UK.

AUTHOR INFORMATION

Corresponding Author

[*]E-mail: susanta.roy@snu.edu.in

Abstaract

This work demonstrates the applicability of one-dimensional nitrogen-doped diamond nanorods (N-DNRs) for the simultaneous electrochemical (EC) detection of Pb^{2+} and Cd^{2+} ions in an electrolyte solution. Well separated voltammetric peaks are observed for Pb^{2+} and Cd^{2+} ions using N-DNRs as a working electrode in square wave anodic stripping voltammetry measurements. Moreover, the cyclic voltammetry response of N-DNR electrodes towards the $Fe(CN)_6^{/4-}$/ $Fe(CN)_6^{/3-}$ redox reaction is better as compared to undoped DNR electrodes. This enhancement of EC performance in N-DNR electrodes is accounted fo by the increased amount of sp^2 bonded nanographitic phases in N-DNR electrodes, enhancing the electrical conductivity at the grain boundary (GB) regions. These findings are supported by transmission electron microscopy and electron energy loss spectroscopy studies. Consequently, the GB defect

induced N-DNRs exhibit better adsorption of metal ions, which makes such samples promising candidates for next generation EC sensing devices.

Keywords: Nitrogen-doped diamond nanorod, cyclic voltammetry, square wave anodic stripping voltammetry, monographitic phase, electron energy loss spectroscopy

1. Introduction

Heavy metal ions (HMIs) are very harmful pollutants in biosphere and due to the development of industries, it turns out to be a very serious issue [1]. The presence of toxic heavy metal ions such as Pb^{2+}, Cd^{2+} etc. in water (sub-micro molar range) can cause severe harmful effects to living organisms [2-4]. The Environmental Protection Agency (EPA) estimates that nearly 20% of the human population was exposed to lead poisoning through contaminated drinking water [5]. Therefore, in order to determine the toxic HMIs in low concentration, a simple, sensitive and accurate detection method is required. So far numerous detection tools have been utilized to detect HMIs, including atomic absorption spectroscopy [6], inductively coupled plasma mass spectroscopy [7], atomic fluorescence spectroscopy [8]. However complicated instrumentation makes these techniques expensive and unsuitable for in-situ analysis. On the other hand, EC techniques are used extensively as an alternative due to their practical advantages such as operational simplicity, good sensitivity, wide linear concentration range with low detection limit, cost effectiveness, miniaturization possibility, and above all, suitable for real time detection [9-13]. The fast, sensitive, selective, precise, low cost EC based sensing in the field of bioelectrochemistry, molecular biology, environmental and pharmaceutical analysis leads to the growth of EC sensors [14-17]. Among many EC methods, anodic stripping voltammetry has been applied most successfully due to its ability to increase the faradic current and reduce the non-faradic current [18-20]. However, the performance of this technique mainly depends on the surface structure, attached chemical functional groups, electrical conductivity, and chemical bonding environment of the electrode

material [21-24]. Another major problem in EC detection is interference due to the presence of other metal ions [11]. Thus, to overcome these problems, there is a need to develop proper electrode materials with the desired chemical functionalities.

In this direction numerous efforts have been made to develop a new kind of advanced electrode materials [10, 21, 23-25]. Much attention has been paid to synthesize carbon based nanostructured materials such as nitrogen doped porous carbon [26], hybrid graphite/diamond films [27], carbon nanotube/diamond core shell nanowires [28], nitrogen-doped carbon nanotubes [29], boron-doped diamond [30], etc. Among these carbonaceous materials, diamond is an exciting material for research due to its fascinating physical properties, such as high hardness, chemical inertness, corrosion resistance and EC stability. Above all, a large EC potential window and good biocompatibility make diamond a promising material for bioelectronics, biosensor, and EC based sensing applications [31-34]. Particularly diamond electrodes synthesized using chemical vapor deposition show excellent EC properties [35-37].

Fabrication of one-dimensional diamond nanostructures (DNSs) and doping with impurities like nitrogen, boron, and phosphorous, appear to be a promising approach to introduce new functionalities with unique structural and electrical activity [38-40]. Especially, incorporation of N or B into diamond leads to a high surface to volume ratio with grain boundary defects due to sp^2 hybridization, resulting in enhanced electrical conductivity with distinct EC properties [33, 41, 42]. Recently, incorporation of N in the growth plasma was shown to lead to an increase in the amorphous phase which in turn converts to a graphitic phase on annealing. These sp^2 contributing defects at the grain boundaries result as an increase in the overall grain boundary (GB) volume, leading to an increase in the density of states at the Fermi level [41, 43]. Such EC biosensing using N and B incorporated DNSs as working electrodes were reported in earlier investigations [23, 24, 44]. Indeed, low and stable capacitive background current, nontoxicity, high chemical stability and high electron transfer capability

make DNS a promising material for sensing biomolecules involved in electron or charge transfer without need for electron mediators [45]. However, the lack of information on the conduction mechanism in DNSs and the unavailability of highly conductive diamond was limiting its application in the field of EC biosensing. Moreover, EC studies of N incorporated DNSs have not yet been explored for the application of simultaneous detection of multiple HMIs.

In this work, we report the applicability of nitrogen-doped diamond nanorods (N-DNRs) as a EC sensor towards the simultaneously detection of lead (Pb^{2+}) and cadmium (Cd^{2+}) ions in an electrolyte solution using square wave anodic stripping voltammetry (SWASV). N-DNRs were fabricated from nitrogen-doped nanocrystalline diamond (N-NCD) films *via* microwave plasma enhanced chemical vapor deposition (MWPECVD) of N-NCD films followed by a reactive ion etching (RIE) process using O_2 gas for the fabrication of nanorods. Undoped DNRs (U-DNRs) fabricated from undoped nanocrystalline diamond (U-NCD) films were also used for comparison. Microstructure and bonding characteristics of N-DNRs were examined using annular dark field (ADF) scanning transmission electron microscopy (STEM) and electron energy loss spectroscopy (EELS). The possible mechanism for the enhancement of the EC performance of N-DNRs for the detection of Pb^{2+} and Cd^{2+} ions is discussed in detail.

2. Results and Discussion

Figures 1a and 1b represent the tilted-view SEM images of U-DNRs and N-DNRs and the insets (I) of Figures 1a and 1b display the plan-view SEM images of U-NCD and N-NCD films. A drastic change in surface morphology from micron-sized grains (inset (I) of Figure 1a) to nano-sized grains (inset (I) of Figure 1b) is observed when nitrogen is incorporated into the CH_4/H_2 plasma during growth process. Figure 1a reveals a random orientation of nanorods in U-DNRs. The U-DNRs were approximately 300 nm in height and about 100 nm in diameter

(inset (II) of Fig. 1a). Due to the presence of nano-sized granular grains in N-NCD films, a smaller diameter with densely packed vertically aligned nanorods were obtained in case of N-DNRs (Figure 1b). The N-DNRs were approximately 500 nm in height and about 50 nm in diameter estimated from the cross-sectional SEM images (inset (II) of Fig. 1b).

The cyclic voltammetry response of U-DNRs and N-DNRs is examined in an aquatic solution of 5 mM $Fe(CN)_6^{3-/4-}$ redox couple containing 0.1 M KCl (Figure 2a). The peak potential separation (ΔE) for N-DNRs was much lower (~ 0.57 V) compared to N-NCD, U-NCD and U-DNRs (ΔE ~ 1 V) electrodes. Also, the peak current value of N-DNRs (curve IV of Figure 2a) is much higher as compared to U-DNRs, N-NCD and U-NCD samples. This low ΔE and high peak current of N-DNRs towards $Fe(CN)_6^{/4-}$/ $Fe(CN)_6^{/3-}$ redox reaction clearly indicates that incorporation of nitrogen in diamond nanorods provides better electron transfer kinetics towards the redox reaction of $Fe(CN)_6^{/4-}$/ $Fe(CN)_6^{/3-}$ as compared to U-DNRs. The better cyclic voltammetric behavior of N-DNRs is correlated with the enhancement of electrical conductivity due to nitrogen incorporation [46, 47]. Thus, nitrogen induced nanorods comprises a larger surface area and low charge transfer resistance, which facilitates the electron transfer kinetics in the electrode surface resulting in a better EC behavior [48] which open up the pathways towards EC based sensing applications.

Figure 2b represents the SWASV analytical characteristics of the as prepared electrode materials where the accumulation process is carried out for 160 s at -1.2 V in 0.1 M acetate buffer (pH=5.0) solution containing 5 µM of Pb^{2+} and Cd^{2+} ions respectively. It is clearly seen that the N-DNR electrode outperforms other electrode materials in terms of stripping peak current response corresponding to the oxidation of Pb^0 and Cd^0 in the SWASV curve. Two prominent peaks can be seen for Pb^{2+} and Cd^{2+} ions having a peak potential at approximately -0.50 V and -0.75 V respectively in the case of N-DNRs sample. Literature [49-52] suggests that the incorporation of nitrogen introduces defects in the sample by creating sp^2 carbon at the

grain boundaries. This grain boundary defect provides good absorbability of metal ions enhancing the accumulation of Pb^{2+} and Cd^{2+} ions on the electrode surface.

In order to obtain the best sensing performance (high sensitivity and low detection limit) from SWASV measurements, we optimized a few experimental parameters such as pH of the electrolyte, deposition potential and deposition time in the acetate buffer solution containing 0.5 µM of each Pb^{2+} and Cd^{2+} ions (see supporting information). The effect of pH on the stripping current response for target HMIs is investigated for the range of 4 to 6 (Figures S1a). A weak voltammetric signal at lower pH value (4 and 4.5) is attributed to the large number of hydrogen ions (H^+) present in the electrolyte which can perturb the electrode surface [10]. When the pH value is high enough (above 5), the current signal begins to decrease possibly due to the hydrolysis of the metal ions [11, 53].The maximum peak current is observed for a pH value of 5. Therefore, the acetate buffer solution of pH = 5 has been used for subsequent experiments. To see the effect of deposition potential on peak current, different scans were executed in the potential range -0.8 V to -1.3 V (Figure S1b). It can be observed that peak current begins to saturate after -1.2 V for both ions and to avoid reasonable generation of H_2 at higher potential we have chosen -1.2 V as the optimized value of the deposition potential for the subsequent experiment [22, 53]. The variation of peak current as a function of deposition time is shown in Figure S1c. A proportional increase in peak current with time can be observed from the graph. The peak current began to saturate after 140 s and to get sufficient accumulation of metal ions on the electrode surface we have selected 160 s as the optimized deposition time for individual and simultaneous detection of Pb^{2+} and Cd^{2+} ions [53].

Under the optimized experimental conditions described above, SWASV has been performed to detect Pb^{2+} and Cd^{2+} ions individually as well as simultaneously using N-DNRs as the working electrode. The SWASV response towards the Pb^{2+} and Cd^{2+} ions with different concentrations is displayed in Figures 3(a–d). SWASV exhibits two well separated peaks

corresponding to the oxidation potential of Cd^0 and Pb^0. The SWASV response for individual detection of trace HMIs is shown in Figure 3a and b. Well-defined voltammetric peaks, proportional to the concentration of Cd^{2+} ions are displayed in Figure 3a for the concentration range 0.01 to 1.1 µM. The linearization equation for this concentration range was found as i/µA = 1.09 + 3.16 c/µM having a correlation coefficient of 0.996 (inset of Figure 3a). The SWASV response of Pb^{2+} ions over a concentration from 0.05 to 1.0 µM is shown in Figure 3b. The linearization equation was obtained as i/µA = 0.05 + 2.52 c/µM with correlation coefficient 0.986 (inset of Figure 3b). These results reveal that we can detect Cd^{2+} and Pb^{2+} ions with a low concentration up to 10 nM and 50 nM experimentally using N-DNRs as a working electrode.

When analyzing both the ions simultaneously, well-defined peaks were observed for the two target metal ions and the peak potential separation was large enough to detect these HMIs selectively and simultaneously as shown in Figure 3c. The linear range was found to be 0.05 to 2 µM for both ions having a correlation coefficient 0.98 for Cd^{2+} and 0.97 for Pb^{2+} respectively. The linearization equations were i/µA = -0.31 + 3.78 c/µM and i/µA = -0.27 + 3.53 c/µM for Cd^{2+} and Pb^{2+} ions respectively (Figure 3d1 and 3d2). These results suggest that we can detect Cd^{2+} and Pb^{2+} ions simultaneously with an experimental detection limit up to 50 nM. A small peak can be seen around -0.4 V potential which possibly points to the formation of some intermetallic compound due to the coexistence of Pb^{2+} and Cd^{2+} ions respectively [53-55]. A comparative study of the performance of our proposed electrode material with other carbon-based nanostructures is given in Table 1.

The N-DNRs sample was utilized as a working electrode material for simultaneous detection of Cd^{2+} and Pb^{2+} ions in an acetate buffer solution. The obtained EC performance is good enough to be implemented for practical applications. However, during simultaneous detection of multiple metal ions there is a possibility for unwanted mutual interference which

may lead to misdetection of the target metal ions. Thus, we focus to study the mutual interference between Cd^{2+} and Pb^{2+} ions in the following section.

Mutual interference is a common issue that occurs during the simultaneous detection of several metal ions. Therefore, we have carried out the mutual interference experiments by increasing one metal ion concentration while keeping the other concentration constant. The effect of Pb^{2+} on the Cd^{2+} stripping peak current is shown in Figure 3e where we fixed the Cd^{2+} ion concentration while increasing the Pb^{2+} ion concentration. A linear increase in peak current of Pb^{2+} ions is observed while the peak current corresponding to Cd^{2+} ions is slightly decreased with an increase in Pb^{2+} ion concentration. The reason is due to the competition between Pb^{2+} and Cd^{2+} ions accumulating at the active sites of N-DNRs, where Pb^{2+} ions may be outcompeted by the Cd^{2+} during the deposition process, as Pb^{2+} ions have a higher diffusivity and more positive reduction potential in comparison to Cd^{2+} ions [56]. In addition there is a possibility of intermetallic compound formation between Cd^{2+} and Pb^{2+} ions which can suppress the Cd^{2+} peak current response. Similar effects have also been reported earlier for the stripping response of Cd^{2+} in the presence of Cu^{2+} ions [57]. Next we investigated the effect of Cd^{2+} ions on the Pb^{2+} stripping peak current by fixing the Pb^{2+} ion concentration with increasing Cd^{2+} ion concentration, as shown in Figure 3f. A significant increment of Pb^{2+} stripping current is observed with increased Cd^{2+} ion concentration. This can be explained by the theoretical model of Schiewe et al. [58] suggesting the possible formation of Cd-Pb intermetallic compound which has the same stripping potential as lead.

To understand the factors responsible for such superior EC behavior of N-DNRs, the microstructure of N-DNRs was investigated using STEM and EELS. Figure 4a displays an ADF- STEM image taken from a single N-DNR. It can be seen that the N-DNR is of cone-like geometry with a diameter varying from ~40 nm at the top, ~60 nm at the middle and ~100 nm at the bottom. Figure 4b shows a high resolution ADF-STEM image of the same nanorod where

structural defects i.e., stacking faults and twins, are clearly visible. To gain insight in the local bonding environment of different carbon atoms present in the N-DNR sample, we have taken an EELS spectrum (Figure 4c) from the region indicated by a yellow rectangle of a typical ADF-STEM image in the inset (I) of Figure 4c. The sp^2 and sp^3 phases were obtained by fitting the experimental spectra to references of graphite and diamond using the EELS model software [59]. The fingerprint of both sp^3 (σ* peak at ~290 eV) and sp^2 (π* peak at ~285 eV) bonding are clearly visible from the EELS spectrum, though it is dominated by sp^3 bonded carbon [60-62].

Moreover, the inset (II) of Figure 4c show the STEM-EELS mapping with sp^3-diamond (D, blue color) and sp^2-graphite (G, yellow color) for the same region depicted in the inset (I) of Figure 4c, reveal the presence of sp^2 and sp^3 phases in the N-DNRs. This observation proves the existence of sp^2 phases in the N-DNRs. On the basis of ADF-STEM and EELS investigations, it is noticed that the N-DNR is a nanohybrid material, which consists of nano-sized diamond grains (sp^3-bonded carbon) along with nanographite (sp^2-bonded carbon) at the grain boundaries of the nanorods. Consequently, the N-DNRs exhibit higher electrical conductivity due to the existence of these nanographitic phases at the grain boundaries.

Thus, the key features for the excellent EC performance of the N-DNRs electrode is due to the presence of nanographitic phases at the GBs. The formation of a nanographitic phase at the GBs (displayed Figure 4) is responsible for the enhanced electron transport of the samples [63]. N impurities are known to be energetically favored at the substitutional sites of the GBs which enhances the electrical conductivity at the GB region [64]. This GB defect caused by N can be used in the large EC potential window with enhanced electron transport kinetics [65]. Thus, the nanographitic phase at the GBs can act as anchor sites to adsorb metal ions on the electrode surface while the enhanced electrical conductivity at the GB region of the N-DNR

electrodes allow a more effective electrodeposition of the metal ions at the negative potentials used; can be responsible for this enhanced sensing performance.

3. Conclusions

In conclusion, we demonstrated a simultaneous detection of Pb^{2+} and Cd^{2+} ions using N-DNRs as electrodes. The SWASV response reveals that N-DNR electrodes show high EC activity towards Pb^{2+} and Cd^{2+} ions in acidic media. Upon optimizing the experimental conditions, we can detect these metal ions up to 10 nM individually and 50 nM simultaneously. The presence of nanographitic phases at the GBs of N-DNRs are held responsible for this high EC activity towards Pb^{2+} and Cd^{2+} ions. In addition, CV results reveal that the N-DNR samples provide a better electron transfer kinetics as compared to N-NCD, U-NCD, and U-DNR electrodes. We have demonstrated a clear picture of surface morphology and microstructural characteristics of N-DNRs, and the EC study suggests that N-DNR electrodes are an excellent choice for simultaneous detection of numerous heavy metal ions.

4. Experimental

4.1. Materials synthesis and characterization

U-NCD and N-NCD films were deposited on polished *n*-type Si substrates using an ASTeX 6500 series MWPECVD system. Prior to diamond growth, the Si substrates were seeded using a water-based state-of-the-art colloidal suspension of 5 nm detonation nanodiamonds (ND) particles (Nano Carbon Institute Co., Ltd.). The U-NCD films were deposited using a CH_4 (1%)/H_2(99%) plasma and N-NCD films were deposited using a CH_4(6%)/H_2(91%)/N_2(3%) plasma while keeping a constant microwave power of 3000 W for 5 h. The pressure and the gas flow rate for the growth of U-NCD and N-NCD films were maintained at 30 Torr and 300 sccm, respectively. Thereafter the pristine films were immersed in the colloidal suspension of ND particles and sonicated for 10 min. These ND particles act as a mask on the film surface which is then subjected to an RIE process using a home-built DC-pulsed sputtering/oxidation

system in an O_2 plasma having a DC power supply of 150 W for 30 min to fabricate U-DNRs and N-DNRs.

Scanning electron microscopy (SEM; FEI Quanta 200 FEG microscope) was used to characterize the morphology of the films and the nanorods. The local microstructure and the bonding characteristics of the N-DNRs were analyzed using a FEI Titan 'cubed' microscope operated at 300 kV for ADF-STEM with the convergence semi-angle α used was 22 mrad and collection semi-angles of the ADF detector laying in the range from 26–60 mrad and EELS in STEM mode. STEM- EELS mapping was carried out making use of Gatan Enfinium EELS spectrometer with a collection semi-angle β=36 mrad .

4.2. Electrochemical measurements

All EC measurements (cyclic voltammetry (CV) and SWASV) were done using an AUTOLAB potentiostat/galvanostat 302N instrument (Metrohm Autolab B.V. Utrecht, Netherlands) controlled by NOVA software. The three electrode setup consists of diamond nanorods as the working electrode, a platinum wire as a counter electrode, and a Ag/AgCl reference electrode.

4.3. Reagents

All chemicals, such as potassium ferrocyanide ($K_4[Fe(CN_6)]$), potassium ferricyanide ($K_3[Fe(CN_6)]$), potassium chloride (KCl) (Fisher scientific) were used as-received without any further purification. Standard solutions of Pb^{2+} and Cd^{2+} ions (1000 ppm each) were purchased from Sigma Aldrich and were diluted further to make solution of desired concentration. All chemicals reagents were of analytical grade. Mili-Q water (18.2MΩ cm) was used in preparation of all aqueous solutions.

Acknowledgements

Sujit Deshmukh indebted to Shiv Nadar University for providing Ph. D. scholarship. The FEI Quanta SEM and Qu-Ant-EM microscope used for the TEM experiments was partly funded by the Hercules fund from the Flemish Government. S. K. and J. V. acknowledge funding from GOA project “Solarpaint” of the University of Antwerp. Kamatchi Jothiramalingam Sankaran is a Postdoctoral Fellow of the Research Foundation-Flanders (FWO).

References

[1] N. Srivastava, C. Majumder, Novel biofiltration methods for the treatment of heavy metals from industrial wastewater, Journal of hazardous materials, 151 (2008) 1-8.

[2] M. Jaishankar, T. Tseten, N. Anbalagan, B.B. Mathew, K.N. Beeregowda, Toxicity, mechanism and health effects of some heavy metals, Interdisciplinary toxicology, 7 (2014) 60-72.

[3] G. Zhu, C.-Y. Zhang, Functional nucleic acid-based sensors for heavy metal ion assays, Analyst, 139 (2014) 6326-6342.

[4] R.A. Bernhoft, Cadmium toxicity and treatment, The Scientific World Journal, 2013 (2013).

[5] I. Oehme, O.S. Wolfbeis, Optical sensors for determination of heavy metal ions, Microchimica Acta, 126 (1997) 177-192.

[6] S. Radi, S. Tighadouini, M. Bacquet, S. Degoutin, F. Cazier, M. Zaghrioui, Y.N. Mabkhot, Organically modified silica with pyrazole-3-carbaldehyde as a new sorbent for solid-liquid extraction of heavy metals, Molecules, 19 (2013) 247-262.

[7] H.-W. Liu, S.-J. Jiang, S.-H. Liu, Determination of cadmium, mercury and lead in seawater by electrothermal vaporization isotope dilution inductively coupled plasma mass spectrometry, Spectrochimica Acta Part B: Atomic Spectroscopy, 54 (1999) 1367-1375.

[8] Z. Wan, Z. Xu, J. Wang, Flow injection on-line solid phase extraction for ultra-trace lead screening with hydride generation atomic fluorescence spectrometry, Analyst, 131 (2006) 141-147.

[9] J.G. Limon-Petersen, I. Streeter, N.V. Rees, R.G. Compton, Voltammetry in weakly supported media: the stripping of thallium from a hemispherical amalgam drop. theory and experiment, The Journal of Physical Chemistry C, 112 (2008) 17175-17182.

[10] X. Xu, G. Duan, Y. Li, G. Liu, J. Wang, H. Zhang, Z. Dai, W. Cai, Fabrication of gold nanoparticles by laser ablation in liquid and their application for simultaneous electrochemical detection of Cd^{2+}, Pb^{2+}, Cu^{2+}, Hg^{2+}, ACS applied materials & interfaces, 6 (2013) 65-71.

[11] Y. Wei, C. Gao, F.-L. Meng, H.-H. Li, L. Wang, J.-H. Liu, X.-J. Huang, SnO_2/reduced graphene oxide nanocomposite for the simultaneous electrochemical detection of cadmium (II), lead (II), copper (II), and mercury (II): an interesting favorable mutual interference, The journal of physical chemistry C, 116 (2011) 1034-1041.

[12] H. Beitollahi, S. Nekooei, Application of a Modified CuO Nanoparticles Carbon Paste Electrode for Simultaneous Determination of Isoperenaline, Acetaminophen and N-acetyl-L-cysteine, Electroanalysis, 28 (2016) 645-653.

[13] H. Beitollahi, S.G. Ivari, M. Torkzadeh-Mahani, Application of antibody–nanogold–ionic liquid–carbon paste electrode for sensitive electrochemical immunoassay of thyroid-stimulating hormone, Biosensors and Bioelectronics, 110 (2018) 97-102.

[14] H. Beitollahi, H. Karimi-Maleh, H. Khabazzadeh, Nanomolar and selective determination of epinephrine in the presence of norepinephrine using carbon paste electrode modified with carbon nanotubes and novel 2-(4-oxo-3-phenyl-3, 4-dihydro-quinazolinyl)-N′-phenyl-hydrazinecarbothioamide, Analytical Chemistry, 80 (2008) 9848-9851.

[15] M.M. Foroughi, H. Beitollahi, S. Tajik, A. Akbari, R. Hosseinzadeh, Electrochemical determination of N-acetylcysteine and folic acid in pharmaceutical and biological samples

using a modified carbon nanotube paste electrode, International Journal of Electrochemical Science, 9 (2014) 8407.

[16] E. Molaakbari, A. Mostafavi, H. Beitollahi, Simultaneous electrochemical determination of dopamine, melatonin, methionine and caffeine, Sensors and Actuators B: Chemical, 208 (2015) 195-203.

[17] H. Beitollahi, F. Garkani Nejad, Graphene oxide/ZnO nano composite for sensitive and selective electrochemical sensing of levodopa and tyrosine using modified graphite screen printed electrode, Electroanalysis, 28 (2016) 2237-2244.

[18] I. Cesarino, E.T. Cavalheiro, C. Brett, Simultaneous Determination of Cadmium, Lead, Copper and Mercury Ions Using Organofunctionalized SBA-15 Nanostructured Silica Modified Graphite–Polyurethane Composite Electrode, Electroanalysis, 22 (2010) 61-68.

[19] M. Li, D.-W. Li, Y.-T. Li, D.-K. Xu, Y.-T. Long, Highly selective in situ metal ion determination by hybrid electrochemical “adsorption–desorption” and colorimetric methods, Analytica chimica acta, 701 (2011) 157-163.

[20] J. Van Staden, M. Matoetoe, Simultaneous determination of copper, lead, cadmium and zinc using differential pulse anodic stripping voltammetry in a flow system, Analytica chimica acta, 411 (2000) 201-207.

[21] C.A. Rusinek, A. Bange, M. Warren, W. Kang, K. Nahan, I. Papautsky, W.R. Heineman, Bare and polymer-coated indium tin oxide as working electrodes for manganese cathodic stripping voltammetry, Analytical chemistry, 88 (2016) 4221-4228.

[22] C. Gao, X.-Y. Yu, R.-X. Xu, J.-H. Liu, X.-J. Huang, AlOOH-reduced graphene oxide nanocomposites: one-pot hydrothermal synthesis and their enhanced electrochemical activity for heavy metal ions, ACS applied materials & interfaces, 4 (2012) 4672-4682.

[23] D. Luo, L. Wu, J. Zhi, Fabrication of boron-doped diamond nanorod forest electrodes and their application in nonenzymatic amperometric glucose biosensing, ACS Nano, 3 (2009) 2121-2128.

[24] J. Shalini, K.J. Sankaran, C.-L. Dong, C.-Y. Lee, N.-H. Tai, I.-N. Lin, In situ detection of dopamine using nitrogen incorporated diamond nanowire electrode, Nanoscale, 5 (2013) 1159-1167.

[25] Z.S. Chu'Er Chng, M. Pumera, A. Bonanni, Doped and undoped graphene platforms: the influence of structural properties on the detection of polyphenols, Scientific reports, 6 (2016) 20673.

[26] L. Cui, J. Wu, H. Ju, Nitrogen-Doped Porous Carbon Derived from Metal–Organic Gel for Electrochemical Analysis of Heavy-Metal Ion, ACS applied materials & interfaces, 6 (2014) 16210-16216.

[27] Y. Guo, N. Huang, B. Yang, C. Wang, H. Zhuang, Q. Tian, Z. Zhai, L. Liu, X. Jiang, Hybrid diamond/graphite films as electrodes for anodic stripping voltammetry of trace Ag+ and Cu^{2+}, Sensors and Actuators B: Chemical, 231 (2016) 194-202.

[28] S.-K. Lee, M.-J. Song, J.-H. Kim, T.-S. Kan, Y.-K. Lim, J.-P. Ahn, D.-S. Lim, 3D-networked carbon nanotube/diamond core-shell nanowires for enhanced electrochemical performance, NPG Asia Materials, 6 (2014) e115.

[29] A. Joshi, T.C. Nagaiah, Nitrogen-doped carbon nanotubes for sensitive and selective determination of heavy metals, RSC Advances, 5 (2015) 105119-105127.

[30] K.E. Toghill, L. Xiao, G.G. Wildgoose, R.G. Compton, Electroanalytical determination of cadmium (II) and lead (II) using an antimony nanoparticle modified boron-doped diamond electrode, Electroanalysis, 21 (2009) 1113-1118.

[31] E.S. Forzani, H. Zhang, W. Chen, N. Tao, Detection of heavy metal ions in drinking water using a high-resolution differential surface plasmon resonance sensor, Environmental science & technology, 39 (2005) 1257-1262.

[32] L.-J. Chen, C.-C. Liu, N.-H. Tai, C.-Y. Lee, W. Fang, I.-N. Lin, Effects of tungsten metal coatings on enhancing the characteristics of ultrananocrystalline diamond films, The Journal of Physical Chemistry C, 112 (2008) 3759-3765.

[33] M. Wei, C. Terashima, M. Lv, A. Fujishima, Z.-Z. Gu, Boron-doped diamond nanograss array for electrochemical sensors, Chemical Communications, (2009) 3624-3626.

[34] A. Härtl, E. Schmich, J.A. Garrido, J. Hernando, S.C. Catharino, S. Walter, P. Feulner, A. Kromka, D. Steinmüller, M. Stutzmann, Protein-modified nanocrystalline diamond thin films for biosensor applications, Nature materials, 3 (2004) 736-742.

[35] S. Raina, W. Kang, J. Davidson, Nanodiamond film with 'ridge'surface profile for chemical sensing, Diamond and Related Materials, 17 (2008) 896-899.

[36] J. Posthill, D. Malta, T. Humphreys, G. Hudson, R. Thomas, R. Rudder, R. Markunas, Method of fabricating a free-standing diamond single crystal using growth from the vapor phase, Journal of applied physics, 79 (1996) 2722-2727.

[37] J. Isberg, J. Hammersberg, E. Johansson, T. Wikström, D.J. Twitchen, A.J. Whitehead, S.E. Coe, G.A. Scarsbrook, High carrier mobility in single-crystal plasma-deposited diamond, Science, 297 (2002) 1670-1672.

[38] W. Janssen, S. Turner, G. Sakr, F. Jomard, J. Barjon, G. Degutis, Y.G. Lu, J. D'Haen, A. Hardy, M.V. Bael, Substitutional phosphorus incorporation in nanocrystalline CVD diamond thin films, physica status solidi (RRL)-Rapid Research Letters, 8 (2014) 705-709.

[39] H. Hsieh, Y. Chang, W. Pong, M.-H. Tsai, F. Chien, P. Tseng, I. Lin, H. Cheng, X-ray-absorption studies of boron-doped diamond films, Applied physics letters, 75 (1999) 2229-2231.

[40] K. Sankaran, N. Tai, I. Lin, Microstructural evolution of diamond films from $CH_4/H_2/N_2$ plasma and their enhanced electrical properties, Journal of Applied Physics, 117 (2015) 075303.

[41] Y. Show, M.A. Witek, P. Sonthalia, G.M. Swain, Characterization and electrochemical responsiveness of boron-doped nanocrystalline diamond thin-film electrodes, Chemistry of materials, 15 (2003) 879-888.

[42] K.J. Sankaran, Y.-F. Lin, W.-B. Jian, H.-C. Chen, K. Panda, B. Sundaravel, C.-L. Dong, N.-H. Tai, I.-N. Lin, Structural and electrical properties of conducting diamond nanowires, ACS applied materials & interfaces, 5 (2013) 1294-1301.

[43] R. Tenne, K. Patel, K. Hashimoto, A. Fujishima, Efficient electrochemical reduction of nitrate to ammonia using conductive diamond film electrodes, Journal of Electroanalytical Chemistry, 347 (1993) 409-415.

[44] J. Shalini, K.J. Sankaran, C.-Y. Lee, N.-H. Tai, I.-N. Lin, An amperometric urea bisosensor based on covalent immobilization of urease on N_2 incorporated diamond nanowire electrode, Biosensors and Bioelectronics, 56 (2014) 64-70.

[45] J. Shalini, K.J. Sankaran, H.-C. Chen, C.-Y. Lee, N.-H. Tai, I.-N. Lin, Mediatorless N 2 incorporated diamond nanowire electrode for selective detection of NADH at stable low oxidation potential, Analyst, 139 (2014) 778-785.

[46] G. Bhattacharya, K.J. Sankaran, S.B. Srivastava, J.P. Thomas, S. Deshmukh, P. Pobedinskas, S.P. Singh, K.T. Leung, M.K. Van Bael, K. Haenen, Probing the flat band potential and effective electronic carrier density in vertically aligned nitrogen doped diamond nanorods via electrochemical method, Electrochimica Acta, 246 (2017) 68-74.

[47] S. Deshmukh, K. Sankaran, K. Srinivasu, S. Korneychuk, D. Banerjee, A. Barman, G. Bhattacharya, D. Phase, M. Gupta, J. Verbeeck, Local probing of the enhanced field electron

emission of vertically aligned nitrogen-doped diamond nanorods and their plasma illumination properties, Diamond and Related Materials, 83 (2018) 118-125.

[48] J. Shalini, Y.-C. Lin, T.-H. Chang, K.J. Sankaran, H.-C. Chen, I.-N. Lin, C.-Y. Lee, N.-H. Tai, Ultra-nanocrystalline diamond nanowires with enhanced electrochemical properties, Electrochimica Acta, 92 (2013) 9-19.

[49] J. Birrell, J. Gerbi, O. Auciello, J. Gibson, D. Gruen, J. Carlisle, Bonding structure in nitrogen doped ultrananocrystalline diamond, Journal of Applied Physics, 93 (2003) 5606-5612.

[50] Y. Chen, N. Tai, I. Lin, Substrate temperature effects on the electron field emission properties of nitrogen doped ultra-nanocrystalline diamond, Diamond and Related Materials, 17 (2008) 457-461.

[51] C.-R. Lin, W.-H. Liao, D.-H. Wei, J.-S. Tsai, C.-K. Chang, W.-C. Fang, Formation of ultrananocrystalline diamond films with nitrogen addition, Diamond and Related Materials, 20 (2011) 380-384.

[52] R. Arenal, P. Bruno, D. Miller, M. Bleuel, J. Lal, D. Gruen, Diamond nanowires and the insulator-metal transition in ultrananocrystalline diamond films, Physical Review B, 75 (2007) 195431.

[53] S. Deshmukh, G. Kandasamy, R.K. Upadhyay, G. Bhattacharya, D. Banerjee, D. Maity, M.A. Deshusses, S.S. Roy, Terephthalic acid capped iron oxide nanoparticles for sensitive electrochemical detection of heavy metal ions in water, Journal of Electroanalytical Chemistry, 788 (2017) 91-98.

[54] A. Ben-Bassat, A. Azrad, Intermetallic compounds formed in mixed (complex) amalgams—I. The systems: copper—mercury, zinc—mercury and copper—zinc—mercury, Electrochimica Acta, 23 (1978) 63-69.

[55] H. Chan, A. Butler, D.M. Falck, M.S. Freund, Artificial neural network processing of stripping analysis responses for identifying and quantifying heavy metals in the presence of intermetallic compound formation, Analytical chemistry, 69 (1997) 2373-2378.

[56] C. Babyak, R.B. Smart, Electrochemical Detection of Trace Concentrations of Cadmium and Lead with a Boron-Doped Diamond Electrode: Effect of KCl and KNO_3 Electrolytes, Interferences and Measurement in River Water, Electroanalysis, 16 (2004) 175-182.

[57] J.A. Wise, D.A. Roston, W.R. Heineman, The effects of Copper-Zinc and Copper-Cadmium intermetallic compounds in different systems used for anodic stripping voltammetry, Analytica Chimica Acta, 154 (1983) 95-104.

[58] J. Schiewe, K.B. Oldham, J.C. Myland, A.M. Bond, V.A. Vicente-Beckett, S. Fletcher, Linear-scan anodic stripping voltammetry with thin-film electrodes: theory of the stripping stage and experimental tests, Analytical Chemistry, 69 (1997) 2673-2681.

[59] J. Verbeeck, S. Van Aert, Model based quantification of EELS spectra, Ultramicroscopy, 101 (2004) 207-224.

[60] S. Prawer, J. Peng, J. Orwa, J. McCallum, D. Jamieson, L. Bursill, Size dependence of structural stability in nanocrystalline diamond, Physical Review B, 62 (2000) R16360.

[61] P. Kovarik, E. Bourdon, R. Prince, Electron-energy-loss characterization of laser-deposited a-C, a-C: H, and diamond films, Physical Review B, 48 (1993) 12123.

[62] A. Dato, V. Radmilovic, Z. Lee, J. Phillips, M. Frenklach, Substrate-free gas-phase synthesis of graphene sheets, Nano letters, 8 (2008) 2012-2016.

[63] Q. Chen, D.M. Gruen, A.R. Krauss, T.D. Corrigan, M. Witek, G.M. Swain, The structure and electrochemical behavior of nitrogen-containing nanocrystalline diamond films deposited from CH4/N2/Ar mixtures, Journal of The Electrochemical Society, 148 (2001) E44-E51.

[64] P. Zapol, M. Sternberg, L.A. Curtiss, T. Frauenheim, D.M. Gruen, Tight-binding molecular-dynamics simulation of impurities in ultrananocrystalline diamond grain boundaries, Physical Review B, 65 (2001) 045403.

[65] S. Bhattacharyya, O. Auciello, J. Birrell, J. Carlisle, L. Curtiss, A. Goyette, D. Gruen, A. Krauss, J. Schlueter, A. Sumant, Synthesis and characterization of highly-conducting nitrogen-doped ultrananocrystalline diamond films, Applied Physics Letters, 79 (2001) 1441-1443.

[66] A. Zeng, E. Liu, S. Tan, S. Zhang, J. Gao, Stripping voltammetric analysis of heavy metals at nitrogen doped diamond-like carbon film electrodes, Electroanalysis, 14 (2002) 1294-1298.

[67] C.E. Banks, M.E. Hyde, P. Tomčík, R. Jacobs, R.G. Compton, Cadmium detection via boron-doped diamond electrodes: surfactant inhibited stripping voltammetry, Talanta, 62 (2004) 279-286.

[68] K.E. Toghill, G.G. Wildgoose, A. Moshar, C. Mulcahy, R.G. Compton, The fabrication and characterization of a bismuth nanoparticle modified boron doped diamond electrode and its application to the simultaneous determination of cadmium (II) and lead (II), Electroanalysis, 20 (2008) 1731-1737.

[69] N. Promphet, P. Rattanarat, R. Rangkupan, O. Chailapakul, N. Rodthongkum, An electrochemical sensor based on graphene/polyaniline/polystyrene nanoporous fibers modified electrode for simultaneous determination of lead and cadmium, Sensors and Actuators B: Chemical, 207 (2015) 526-534.

[70] E. Nurhayati, Y. Juang, M. Rajkumar, C. Huang, C.-C. Hu, Effects of dynamic polarization on boron-doped NCD properties and on its performance for electrochemical-analysis of Pb (II), Cu (II) and Hg (II) in aqueous solution via direct LSV, Separation and Purification Technology, 156 (2015) 1047-1056.

[71] L. Li, D. Liu, A. Shi, T. You, Simultaneous stripping determination of cadmium and lead ions based on the N-doped carbon quantum dots-graphene oxide hybrid, Sensors and Actuators B: Chemical, (2017).

Figure captions:

Figure 1. Tilt-view SEM micrographs of (a) U-DNRs and (b) N-DNRs. The insets of Fig. 1 are: (I) the plan-view SEM micrographs of U-NCD and N-NCD film and (II) the cross-sectional SEM micrographs of U-DNRs and N-DNRs respectively.

Figure 2. (a) Cyclic voltammetry response of (I) U-NCD (II) N-NCD (III) U-DNRs and (IV) N-DNRs in the solution of 5 mM $Fe(CN)_6^{3-/4-}$ containing 0.1 M KCl. (b) SWASV response of (I) U-NCD (II) N-NCD (III) U-DNRs and (IV) N-DNRs towards the simultaneous detection 5 µM of each Pb^{2+} and Cd^{2+} ions in 0.1 M acetate buffer solution having pH value of 5. The experimental parameters are as follows: deposition time =160 s, deposition potential = -1.2 V, amplitude = 25 mV, step potential = 4 mV and frequency = 25 Hz

Figure 3. SWASV response of N-DNRs for the individual detection of (a) Cd^{2+} ions over a concentration range 0.01 – 1.1 µM and (b) Pb^{2+} ions over a concentration range 0.05–1.0 µM. Inset of figure (a) and (b) shows the linear calibration plot of peak current as a function Cd^{2+} and Pb^{2+} ions concentration respectively. (c) SWASV response of N-DNR for the simultaneous detection of Cd^{2+} and Pb^{2+} ions over a concentration range 0.05 – 2 µM. (d_1 and d_2) linear calibration plot of Cd^{2+} and Pb^{2+} ion corresponding to panel c. SWASV response of N-DNR at (e) 1.5, 2, 2.5, 3 µM of Pb^{2+} in the presence of 1 µM Cd^{2+} (f) 1, 1.5, 2 µM of Cd^{2+} in the presence of 0.5 µM of Pb^{2+}. Experimental conditions of SWASV are identical to fig 2.

Figure 4. (a) Typical cross-sectional ADF-STEM micrograph of N-DNRs. (b) Typical HAADF STEM micrograph which is taken from a single nanorod. (c) Monochromated core-loss EELS spectrum taken from the region indicated by the yellow rectangle in inset (I), the acquisition was proceeded on Titan FEI at 120 kV with energy resolution of approximately 150 meV. The inset (II) shows the EELS abundance map for σ* (blue) and π* (yellow).

Table 1. Comparison of the detection limit and the linear range of nitrogen doped diamond nanorods with other carbon based nanostructured electrode materials for the detection of Pb^{2+} and Cd^{2+} ions.

Electrode material	Detection limit (µM)		Linear Range (µM)	
	Pb^{2+}	Cd^{2+}	Pb^{2+}	Cd^{2+}
Antimony nanoparticles modified boron doped diamond electrode [30]	0.12	0.34	0.2 – 2.41	0.4 – 4.4
Nitrogen doped diamond like carbon film [66]	0.076	–	0.5 - 2	–
Boron doped diamond [67]	–	0.0039	–	0.25 – 0.3
Bismuth nanoparticle modified boron doped diamond electrode [68]	0.01	0.016	0.09 – 0.9	0.17 – 1.779
Graphene/polyaniline/polystyrene nanoporous fibre [69]	0.016	0.04	0.048 – 2.41	0.08 – 4.44
Boron doped monocrystalline diamond [70]	1.339	–	1 – 22.5	–
N-doped carbon quantum dots graphene oxide hybrid [71]	0.005	0.06	0.1 - 50	0.09 – 99.99
Nitrogen doped diamond nanorods (Present work)	0.05 (expt.)	0.01 (expt.)	0.05 -1	0.01 – 1.1

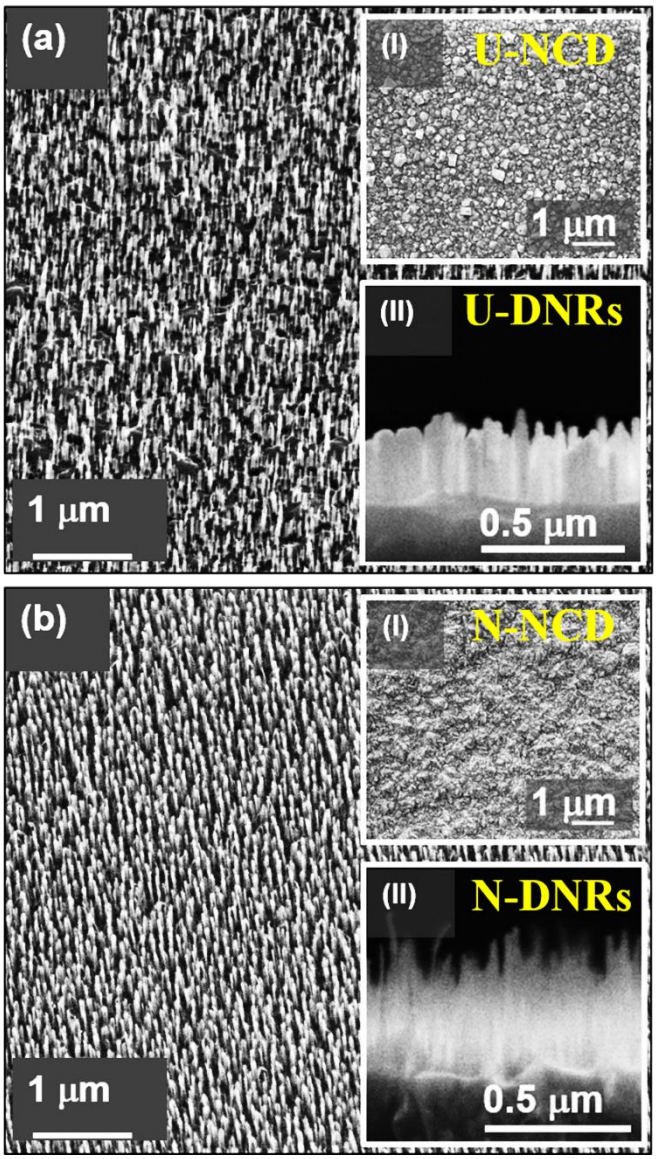

Figure 1.

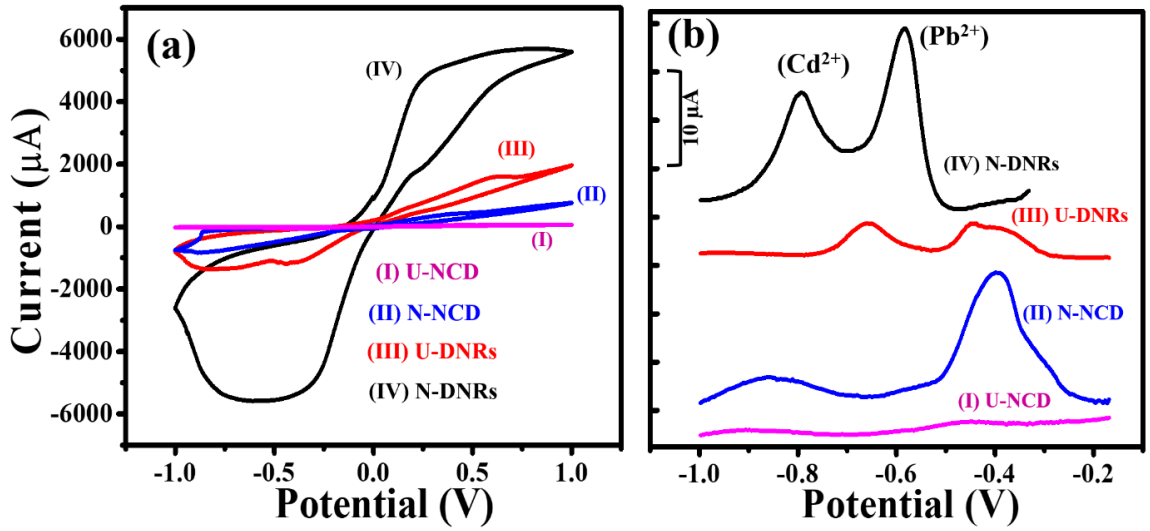
(a)
(IV)
(III)
(II)
(I)
(I) U-NCD
(II) N-NCD
(III) U-DNRs
(IV) N-DNRs
Current (μA)
Potential (V)
(b)
(Cd2+)
(Pb2+)
10 μA
(IV) N-DNRs
(III) U-DNRs
(II) N-NCD
(I) U-NCD
Potential (V)

Figure 2.

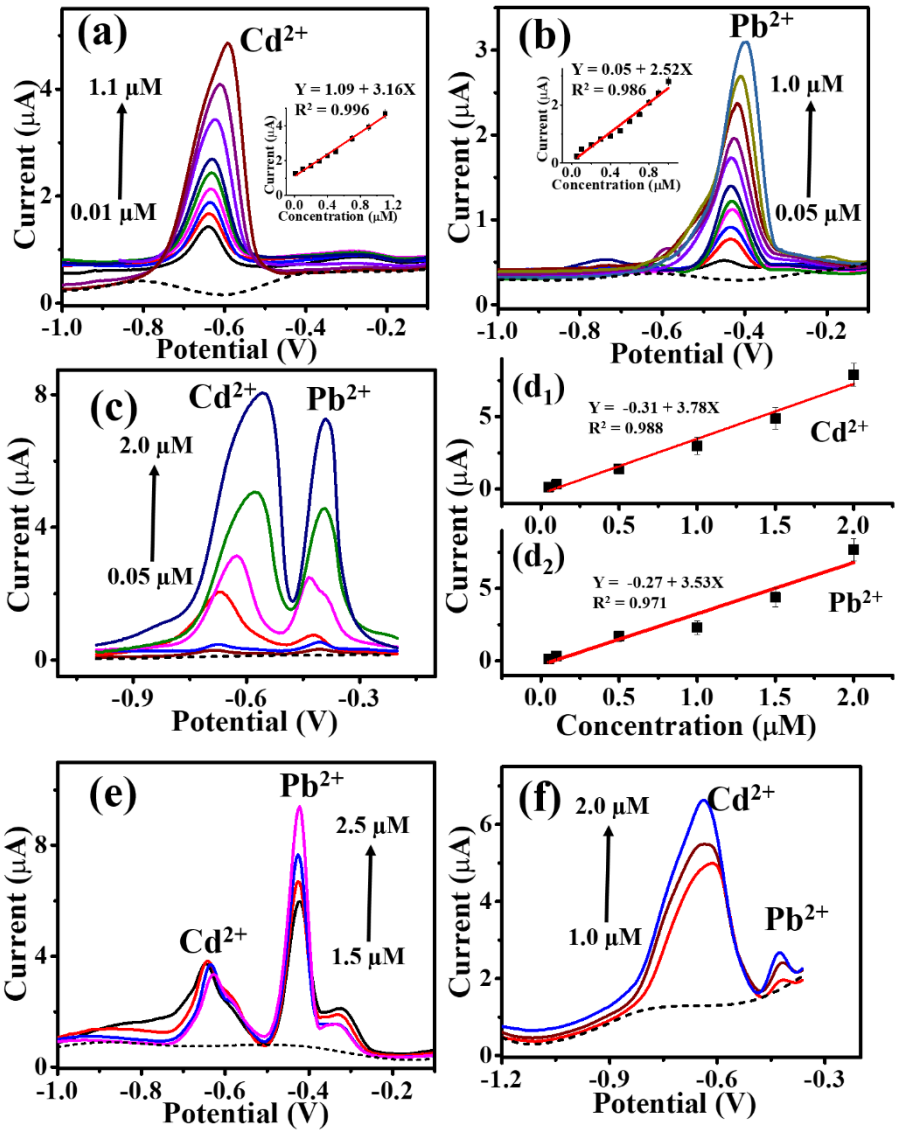
(a)
Cd2+
1.1 µM
0.01 µM
Y = 1.09 + 3.16X
R² = 0.996
Current (µA)
Concentration (µM)
Potential (V)
(b)
Pb2+
1.0 µM
0.05 µM
Y = 0.05 + 2.52X
R² = 0.986
(c)
Cd2+
Pb2+
2.0 µM
0.05 µM
(d1)
Y = -0.31 + 3.78X
R² = 0.988
Cd2+
(d2)
Y = -0.27 + 3.53X
R² = 0.971
Pb2+
Concentration (µM)
(e)
Pb2+
2.5 µM
1.5 µM
Cd2+
(f)
2.0 µM
1.0 µM
Cd2+
Pb2+

1

2 **Figure 3.**

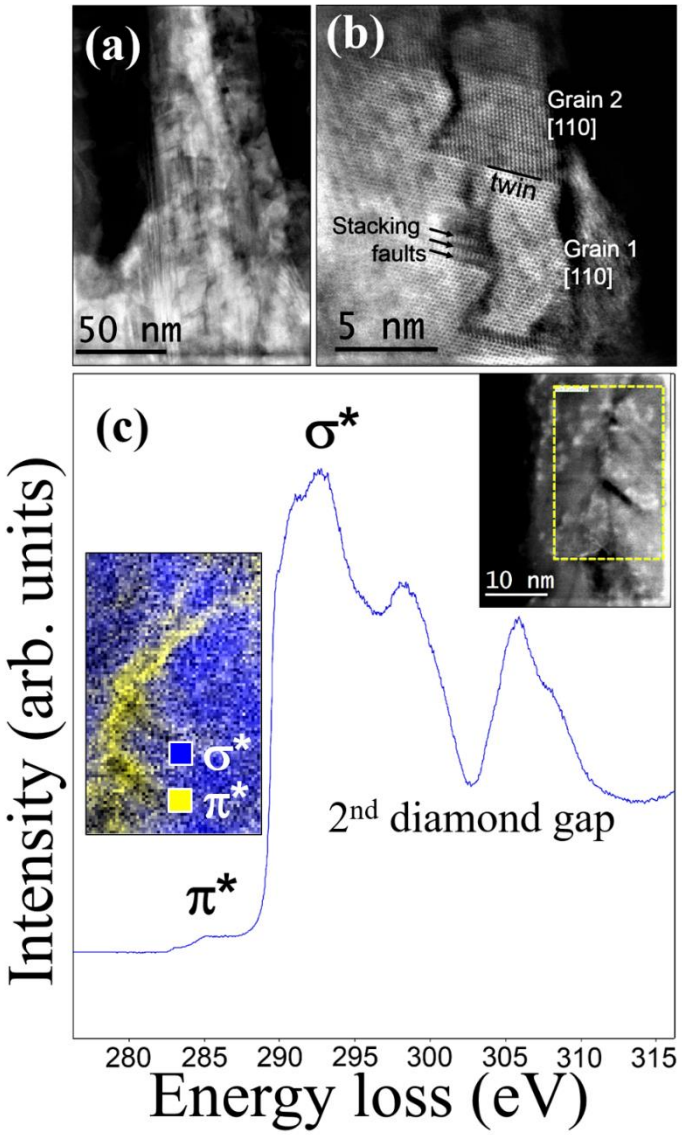
(a)
50 nm
(b)
Grain 2
[110]
twin
Stacking
faults
Grain 1
[110]
5 nm
(c)
σ*
10 nm
σ*
π*
π*
2nd diamond gap
Intensity (arb. units)
280
285
290
295
300
305
310
315
Energy loss (eV)

Figure 4.